Sensitivity Enhancement System for Pulse Compression Weather Radar

CUONG M. NGUYEN AND V. CHANDRASEKAR

Colorado State University, Fort Collins, Colorado

(Manuscript received 13 February 2014, in final form 17 July 2014)

ABSTRACT

The use of low-power solid-state transmitters in weather radar to keep costs down requires a pulse compression technique that maintains an adequate minimum detectable signal. However, wideband pulse compression filters will partly reduce the system's sensitivity performance. In this paper, a sensitivity enhancement system (SES) for pulse compression weather radar is developed to mitigate this issue. SES uses a dual-waveform transmission scheme and an adaptive pulse compression filter. The waveforms' diversity can be done in the frequency domain or the time domain. The adaptive filter is designed based on the self-consistency between signal returns from the two waveforms. Analysis based on radar-simulated data and observations from NASA's dual-frequency dual-polarized Doppler radar (D3R) shows that by using SES, the system sensitivity can be improved by 7–10 dB when compared to that of the conventional matched filter.

1. Introduction

Sensitivity is a critical aspect of any radar system. It is especially critical for weather radar because the system is supposed to detect intense reflectivity patterns as well as precisely measure relatively weak precipitation echoes. This aspect is even more imperative for electronically scanned phased array weather radar because the peak transmit power is usually lower. Modern active phased array antennas include many elements in which each has its own transmit and receive modules. To keep costs down, low-power solid-state transmitters are used at each element. The primary disadvantage of these transmitters is low peak power. This is because the weather radar sensitivity is inversely proportional to the product of pulse width and peak power (Bringi and Chandrasekar 2001). However, solid-state transmitters have relaxed restrictions on the duty circle that allow implementation of pulse compression techniques in order to obtain acceptable sensitivity for weather observations.

Pulse compression is a technique that allows a radar system to transmit a long coded waveform and compress the received echo to obtain a narrow pulse. The primary objective of the pulse compression technique is to improve range resolution and sensitivity while avoiding transmission of higher peak power. This technology has been widely used in military and air traffic control radar systems since the early 1950s and is described in the literature (Skolnik 2002). However, the use of pulse compression in ground-based weather radar to study precipitation targets is very limited. In the early 1970s, Fletter demonstrated a 7-bit Barker phase-coded pulse on the coherent FPS-18 radar at McGill University (Fetter 1970). Bucci and Urkowitz (1993), Keeler (1995), and Mudukutore et al. (1998) have presented technical and engineering aspects of this application. Recently, frequency diversity pulse compression waveforms have been implemented and demonstrated in the Ku–Ka-band National Aeronautics and Space Administration (NASA) dual-frequency dual-polarized Doppler radar (D3R) (Chandrasekar et al. 2010). In this work, system sensitivity, a critical aspect of pulse compression technique for weather targets, has been studied.

In a pulse compression weather radar, the transmit pulse has a long duration and wide bandwidth. A long pulse width is needed to increase measurement sensitivity. For example, with the same peak/average

Corresponding author address: Cuong M. Nguyen, Electrical and Computer Engineering, Colorado State University, 1373 Campus Delivery, Fort Collins, CO 80523-1373.
E-mail: cmnguyen@engr.colostate.edu

DOI: 10.1175/JTECH-D-14-00049.1

Publisher's Note: This article was revised on 30 December 2014 to include a final sentence in the Acknowledgments section that was left out when originally published.

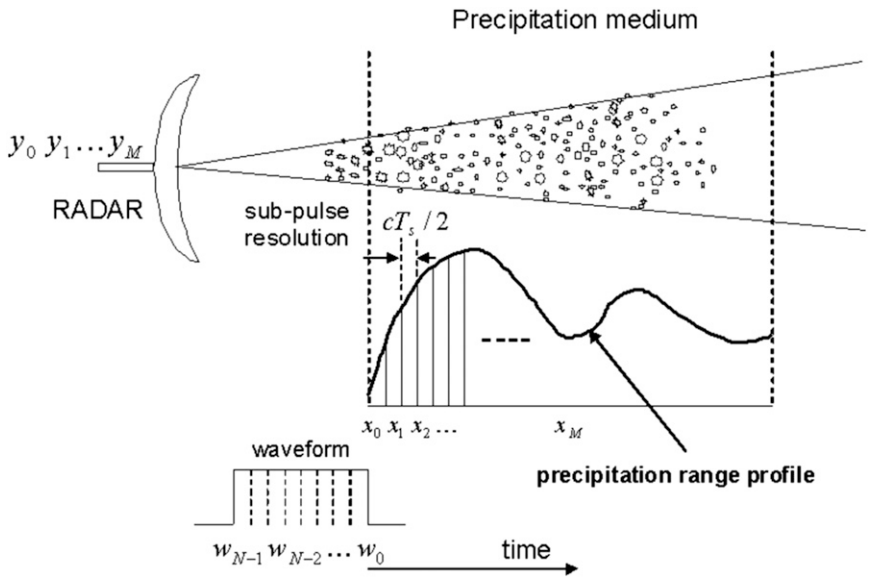

FIG. 1. Pulse compression discrete signal model.

transmitted power, a system using a 40-μs pulse width is nearly 15 dB more sensitive than one transmitting a pulse of 1-μs width. To get improved range resolution, the wideband signal is vital; however, it comes with a major drawback. Because the receiver noise is proportional to the bandwidth, a wider band receiver would introduce more noise into the system, thereby decreasing system sensitivity. For instance, a linear-frequency-modulated waveform system using a Taylor mismatch filter designed for a peak sidelobe level (PSL) of 38 dB would require a time-bandwidth product (BT) of 400 (RCA 1965). Thus, if 40-μs pulses are used, then the transmitted signal bandwidth has to be at least 10 MHz. When compared to a system using uncoded pulses of 1-MHz bandwidth, the system noise increases by 10 dB. Consequently, the system sensitivity is decreased by 10 dB. To overcome this problem, one might think of using a conventional low-pass filter (LPF) to remove the noise at the receiver. However, because of inherent properties of the wideband signal and the white noise, employing any LPF at the receiver to reduce noise will also increase the filter loss. Hence, improving the system sensitivity using such standard techniques is not useful.

In this work, a sensitivity enhancement system (SES) for pulse compression weather radars is introduced. SES utilizes a transmission scheme with two different waveforms that is implemented such that both waveforms will measure the same precipitation volume. At the receiver, an adaptive filter is designed based on the self-consistency between signals from the waveforms. The signal from the second waveform is estimated at each range gate using knowledge of the medium obtained from the first waveform. The SES processing is an enhancement of the conventional pulse compression techniques, and it is able to improve the system sensitivity significantly as well as provide very good Doppler tolerance and PSL performance.

This paper is organized as follows. The discrete signal model for pulse compression weather radar is presented in section 2. The sensitivity enhancement system, including filter design and a Doppler compensation technique, is described in section 3. Section 4 will introduce a dual-waveform transmission scheme for SES. The evaluation of the new filter based on signal simulation with various input parameters is discussed in section 5. Also in this section, a comparison between sensitivities by SES and a matched filter system is given. Next, in section 6, NASA D3R pulse compression radar data are used to demonstrate the performance of SES. The last section discusses and summarizes important results of this paper.

2. Signal model

Consider a pulse compression radar system with a sampling frequency of F_s. The corresponding sampling time is $T_s = 1/F_s$. The range resolution corresponding to the subpulse is $r = cT_s/2$, where c is the velocity of light in a vacuum. For example, a system with a 10-MHz chirp gives a subpulse range resolution of 15 m. Figure 1 shows a signal transmission model

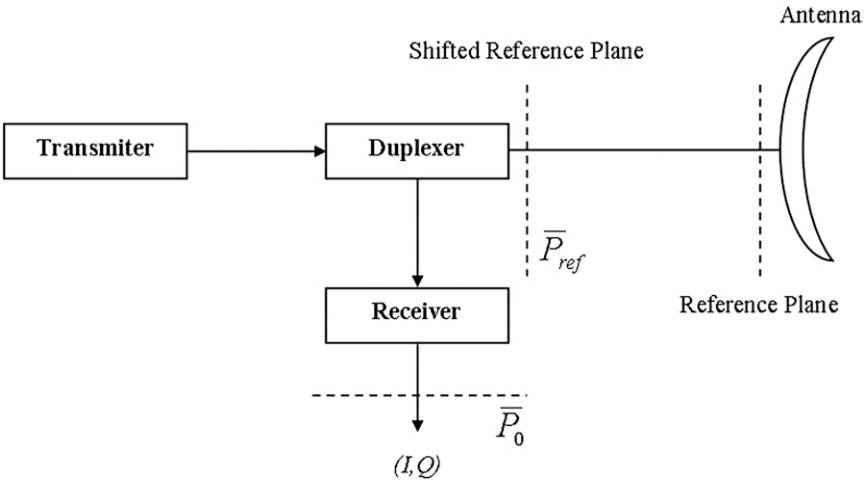

FIG. 2. Illustrating the shifted reference plane for reflectivity calculation (Bringi and Chandrasekar 2001).

where both the precipitation range profile and the transmitted waveform are sampled at frequency F_s. The range profile is represented by a vector of contiguous samples $\mathbf{x} = (x_0, x_1, \ldots, x_M, \ldots)$, where x_i is the signal from the ith range gate.

According to Bringi and Chandrasekar (2001), the received signal is a convolution of the medium and transmitted waveform. Denoting a N-length vector $\mathbf{w} = (w_0, w_1, \ldots, w_{N-1})^{\mathrm{T}}$ as a transmit waveform, the received signal at the antenna port is expressed by

$$\mathbf{y} = \mathbf{x} * \mathbf{w} + \boldsymbol{\eta}, \tag{1}$$

where the asterisk ($*$) denotes the convolution operator and $\boldsymbol{\eta}$ is the noise vector.

The convolution [Eq. (1)] can be expressed in a matrix form,

$$\begin{bmatrix} y_0 \\ y_1 \\ y_2 \\ \vdots \\ y_{M-1} \\ y_M \end{bmatrix} = \begin{bmatrix} x_0 & 0 & \cdots & 0 \\ x_1 & x_0 & \cdots & 0 \\ x_2 & x_1 & \cdots & 0 \\ \vdots & \vdots & & \vdots \\ x_{M-1} & x_{M-2} & \cdots & x_{M-N} \\ x_M & x_{M-1} & \cdots & x_{M-N+1} \end{bmatrix} \begin{bmatrix} w_0 \\ w_1 \\ w_3 \\ \vdots \\ w_{N-1} \end{bmatrix} + \begin{bmatrix} \eta_0 \\ \eta_1 \\ \eta_2 \\ \vdots \\ \eta_{M-1} \\ \eta_M \end{bmatrix}, \tag{2}$$

For $n \geq N-1$ we define a processing window $[n-N+1, n+N-1]$ as

$$\begin{bmatrix} y_n \\ y_{n+1} \\ \vdots \\ y_{n+N-1} \end{bmatrix} = \begin{bmatrix} x_n & x_{n-1} & \cdots & x_{n-N+1} \\ x_{n+1} & x_n & \cdots & x_{n-N+2} \\ \vdots & \vdots & \ddots & \vdots \\ x_{n+N-1} & x_{n+N-2} & \cdots & x_n \end{bmatrix} \begin{bmatrix} w_0 \\ w_1 \\ \vdots \\ w_{N-1} \end{bmatrix} + \begin{bmatrix} \eta_n \\ \eta_{n+1} \\ \vdots \\ \eta_{n+N-1} \end{bmatrix} \tag{3}$$

or in short notation as

$$\mathbf{y}_n = \mathbf{X}_n \mathbf{w} + \boldsymbol{\eta}_n, \tag{4}$$

where $\mathbf{X}$ denotes the $N \times N$ matrix in Eq. (3) and $\boldsymbol{\eta}_n$ is an additive white noise vector within the processing window, $\boldsymbol{\eta}_n \sim N(0, \sigma_N^2 \mathbf{I}_n)$, σ_N^2 is noise power, and $\mathbf{I}_n$ is an identity matrix.

3. SES

a. Sensitivity of pulse compression weather radar

The reflectivity is estimated from the received power at the shifted reference plane (Fig. 2). The reflectivity is given by

$$Z_e = C' R^2 \overline{P}_{\mathrm{ref}}. \tag{5}$$

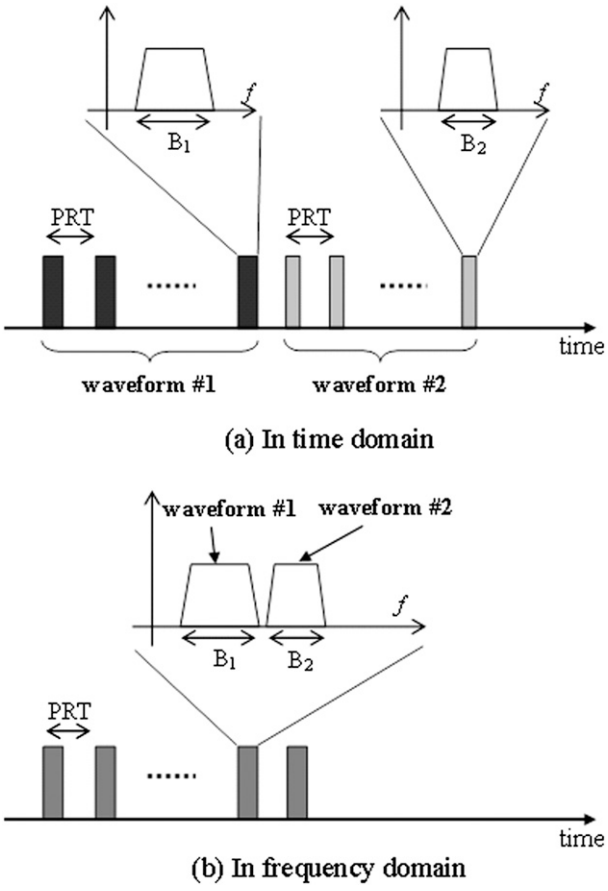

FIG. 3. SES dual-waveform transmission scheme.

In Eq. (5), P_{ref} is the received power at the reference port, R is the radar range, and C' is a constant given by

$$C' = \frac{1}{\pi^5 |K_w|^2}\left(\frac{2}{c\tau}\right)\left[\frac{(4\pi^3 l_{wg}^2)}{P_t G_0^2}\right]\left(\frac{8\ln 2}{\pi\theta_B\varphi_B}\right)\lambda^2. \quad (6)$$

The power at the reference plane is related to the power at the output of the receiver by $\overline{P}_{\text{ref}} = (l_r/G_r)\overline{P}_0$, where l_r is the filter loss and G_r is the receiver gain (Bringi and Chandrasekar 2001). Hence, the equivalent reflectivity can be computed from the receiver output power using

$$Z_e = CR^2\overline{P}_0, \quad (7)$$

where

$$C = \frac{1}{\pi^5 |K_w|^2}\left(\frac{2}{c\tau}\right)\left(\frac{l_r}{G_r}\right)\left[\frac{(4\pi^3 l_{wg}^2)}{P_t G_0^2}\right]\left(\frac{8\ln 2}{\pi\theta_B\varphi_B}\right)\lambda. \quad (8)$$

TABLE 1. Pulse compression simulation input parameters.

Parameters	Values
Frequency (GHz)	13.91
Antenna gain (dB)	44.5
3-dB beamwidth (°)	1
Peak transmit power (W)	100
Sampling frequency (f_s; MHz)	5
Waveform 1 pulse width (μs)	40
Waveform 2 pulse width (μs)	40
Waveform 1 bandwidth (MHz)	3.6
Waveform 2 bandwidth (MHz)	2.5
Noise figure (dB)	4.5
Spectrum width (m s^{-1})	2
Integration circle (samples)	128

The unit of Z_e is square millimeters per meter. In practice, this is expressed in decibel scale (dBZ). The radar equation can now be written as

$$Z_e(\text{dB}Z) = \overline{P}_0(\text{dB}m) + C(\text{dB}) + 20\log[R(\text{km})]. \quad (9)$$

The above-mentioned equations are explained in detail in Bringi and Chandrasekar (2001).

It is customary to define the minimum detectable reflectivity Z_e at a given range R when the signal-to-noise ratio (SNR) is unity; that is, $\overline{P}_0 = P_N = kTB$, where B is the receiver-equivalent noise bandwidth. Equation (9) can be rewritten as

$$\min(Z_e)(\text{dB}Z) = 10\log_{10}(kTB) + C(\text{dB}) + 20\log[R(\text{km})] \quad (10)$$

The radar sensitivity is studied in terms of the minimum reflectivity (Bringi and Chandrasekar 2001).

Equations (8) and (10) suggest several ways to improve system sensitivity. While the option of increasing the transmit peak power is limited by the use of low-power solid-state transmitters, designing a better pulse compression filter for sensitivity enhancement is a potential solution. An intuitive way to do this is to narrow the receiver filter bandwidth to reduce the product kTB (10). However, given the fact that a pulse compression waveform is a wideband signal, reducing the filter bandwidth results in increasing the filter loss l_r (Bringi and Chandrasekar 2001) and therefore, it degrades the system sensitivity performance. In addition, a narrower filter bandwidth will lead to a larger output's range resolution that may be unacceptable for many applications.

It is known that the received radar returns ($\mathbf{y}_n$) include convolutional components involving samples of $\mathbf{X}_n$ prior to and after the nth gate. Conventional pulse compression filters such as matched filter and mismatched filter do

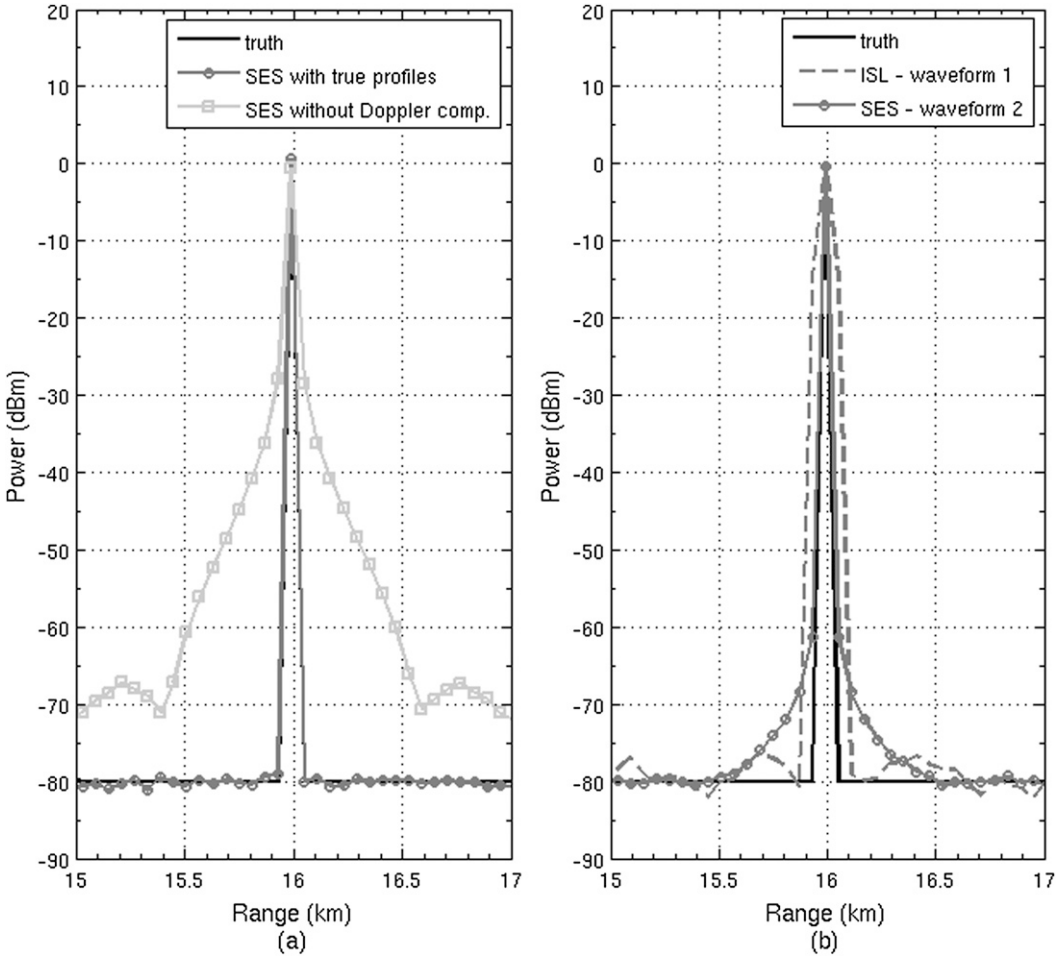

FIG. 4. Effect of Doppler in SES processing. (a) True power profile is used: Doppler compensation is done with known velocity (dark gray curve) and no Doppler compensation (light gray curve). (b) Doppler compensation is done with power, and velocity profiles are obtained from the first waveform.

not account for this characterization. As a result, when a significantly large signal is present within the $(N - 1)$ range gates prior to or after sample x_n, the performance of those filters can deteriorate. In addition, the received signal from precipitation is the sum of the contribution from a large number of hydrometeor particles extending over a large range with different scattering amplitudes and moving with different velocities. In general, it is not a scaled, time-shifted replica of the transmit waveform and therefore, a conventional pulse compression–matched filter may not always provide an optimal SNR. Those shortcomings suggest that it is necessary to obtain an adaptive filter for the received signals of a pulse compression weather radar. The filter's coefficients should be able to adapt to the distribution of signal density over the measurement range and also be able to account for the Doppler shift effect. The remainder of this paper develops a novel system called SES for pulse compression weather radar that significantly improves system sensitivity while maintaining robust estimates of signal parameters.

b. Signal covariance matrix

For precipitation targets, signals from different range gates are zero mean and uncorrelated. The covariance matrix of the measured signal can be represented as

$$\begin{aligned}\mathbf{R}_{\mathbf{yy}} &= E(\mathbf{y}_n\mathbf{y}_n^{\mathrm{H}}) = E[(\mathbf{X}_n\mathbf{w} + \boldsymbol{\eta}_n)(\mathbf{X}_n\mathbf{w} + \boldsymbol{\eta}_n)^{\mathrm{H}}] \\ &= E[\mathbf{X}_n(\mathbf{w}\mathbf{w}^{\mathrm{H}})\mathbf{X}_n^{\mathrm{H}}] + E(\boldsymbol{\eta}_n\boldsymbol{\eta}_n^{\mathrm{H}}) \\ &= E(\mathbf{X}_n\mathbf{W}\mathbf{X}_n^{\mathrm{H}}) + \sigma_N^2\mathbf{I}_n \\ &= \sum_{k=-(N-1)}^{N-1} p_{n+k}\mathbf{W}_k + \sigma_N^2\mathbf{I}_n, \end{aligned} \tag{11}$$

where the superscript H denotes Hermitian and p_{n+k} is the signal power at gate $(n+k)$th. Expression $\mathbf{W} = \mathbf{w}\mathbf{w}^{\mathrm{H}}$ and $\mathbf{W}_k$ is a shifted version of $\mathbf{W}$ by k elements and the rest is zero padded. We denote $\mathbf{W}_k = \mathrm{circ}(\mathbf{W}, k)$. If k is positive, then the values of $\mathbf{W}$ are shifted down and right. If k is negative, then the values of $\mathbf{W}$ are shifted up and left. For example,

$$\mathbf{W}_1 = \mathrm{circ}(\mathbf{W}, 1) = \begin{bmatrix} 0 & 0 & \cdots & 0 \\ 0 & w_{1,1} & \cdots & w_{1,N-1} \\ \vdots & \vdots & \ddots & \vdots \\ 0 & w_{N-1,1} & \cdots & w_{N-1,N-1} \end{bmatrix} \tag{12a}$$

$$\mathbf{W}_{-1} = \mathrm{circ}(\mathbf{W}, -1) = \begin{bmatrix} w_{2,2} & \cdots & w_{2,N} & 0 \\ \vdots & \ddots & \vdots & \vdots \\ w_{N,2} & \cdots & w_{N,N} & 0 \\ 0 & \cdots & 0 & 0 \end{bmatrix}. \tag{12b}$$

For $m \le N-1$, denote $\mathbf{x}_m = (x_{n-m}, x_{n-m+1}, \ldots, x_{n+m-1}, x_{n+m})^{\mathrm{T}}$ and its covariance matrix is expressed as

$$\mathbf{R}_{\mathbf{xx}} = E(\mathbf{x}_m \mathbf{x}_m^{\mathrm{H}}) = \begin{bmatrix} p_{n-m} & 0 & \cdots & 0 \\ 0 & p_{n-m+1} & \cdots & 0 \\ \vdots & \vdots & \ddots & \vdots \\ 0 & 0 & \cdots & p_{n+m} \end{bmatrix}. \tag{13}$$

Note the signal covariance matrix is only defined by power samples of the medium.

c. SES processing

In this section, we derive the estimator of the unobserved vector $\mathbf{x}_m$ on the basis of observed vector $\mathbf{y}_n$. By definition,

$$\hat{\mathbf{x}}_m = \arg\max_{\mathbf{x}_m} f_{\mathbf{Y}|\mathbf{X}}(\mathbf{y}_n \,|\, \mathbf{x}_m) f_{\mathbf{X}}(\mathbf{x}_m), \tag{14}$$

where $f_{\mathbf{Y}|\mathbf{X}}$ is the probability distribution of $\mathbf{y}_n$ given $\mathbf{x}_m$ and $f_{\mathbf{X}}$ is the prior distribution of $\mathbf{x}_m$. The distributions of the weather radar signals are multivariate normal (Bringi and Chandrasekar 2001) and therefore,

$$f_{\mathbf{X}}(\mathbf{x}_m) = \frac{1}{(2\pi)^{(2m+1)/2}\det(\mathbf{R}_{\mathbf{xx}})} \exp\left\{-\frac{1}{2}\mathbf{x}_m^{\mathrm{H}}\mathbf{R}_{\mathbf{xx}}^{-1}\mathbf{x}_m\right\} \tag{15a}$$

$$f_{\mathbf{Y}|\mathbf{X}}(\mathbf{y}_n \,|\, \mathbf{x}_m) = \frac{1}{(2\pi)^{N/2}\det(\mathbf{R}_{zz})} \exp\left[-\frac{1}{2}(\mathbf{y}_n - \mathbf{S}_m\mathbf{x}_m)^{\mathrm{H}}\mathbf{R}_{zz}^{-1}(\mathbf{y}_n - \mathbf{S}_m\mathbf{x}_m)\right], \tag{15b}$$

where $\mathbf{R}_{\mathbf{xx}}$ is described in Eq. (13) and $\mathbf{R}_{zz}$ is the covariance matrix of $\mathbf{z} = \mathbf{y}_n - \mathbf{S}_m\mathbf{x}_m$,

$$\mathbf{R}_{zz} = \sum_{\substack{k=-(N-1) \\ |k|>m}}^{N-1} p_{n+k}\mathbf{W}_k + \sigma_N^2\mathbf{I}_N \tag{16}$$

$$\mathbf{S}_m = \begin{bmatrix} w_m & w_{m-1} & \cdots & w_0 & 0 & \cdots & 0 \\ w_{m+1} & w_m & \cdots & w_1 & w_0 & \cdots & 0 \\ \vdots & \vdots & \ddots & \vdots & \vdots & \ddots & \vdots \\ 0 & 0 & \cdots & w_{N-1} & w_{N-2} & \cdots & w_{N-m-1} \end{bmatrix}. \tag{17}$$

Substituting Eqs. (15), (16), and (17) in (14), taking the derivative with respect to $\mathbf{x}_m$ and solving for minima, we obtain the estimator for $\mathbf{x}_m$ in a closed-form expression,

$$\hat{\mathbf{x}}_m = (\mathbf{S}_{\mathrm{H}}^m\mathbf{R}_{zz}^{-1}\mathbf{S}_m + \mathbf{R}_{\mathbf{xx}}^{-1})^{-1}\mathbf{S}_m^{\mathrm{H}}\mathbf{R}_{zz}^{-1}\mathbf{y}_n. \tag{18}$$

The solution (18) has the form $\hat{\mathbf{x}}_m = \mathbf{F}\mathbf{y}_n$, where

$$\mathbf{F} = (\mathbf{S}_m^{\mathrm{H}}\mathbf{R}_{zz}^{-1}\mathbf{S}_m + \mathbf{R}_{\mathbf{xx}}^{-1})^{-1}\mathbf{S}_m^{\mathrm{H}}\mathbf{R}_{zz}^{-1} \tag{19}$$

is termed the adaptive filter for SES.

d. Doppler compensation

The analysis described in the above section does not include the impact of Doppler shift. It simply assumes that the Doppler shifts of the samples $\mathbf{x}_m$ are equal to zero. Although the gradient in radial Doppler shifts of weather targets is not as high as that in the case of military targets, it may still affect the filter performance, especially where a weather radar system is required to measure weather signals accurately. For example, a strong and fast-moving storm may heavily contaminate nearby weak

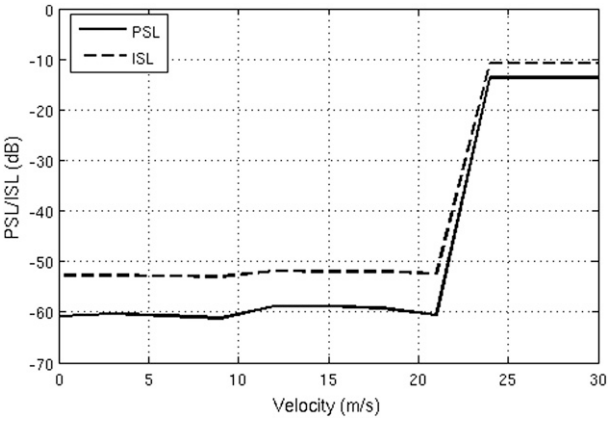

FIG. 5. Sidelobe level as a function of Doppler velocity. Performance of SES decreases when velocity exceeds Nyquist velocity ($v_a = 21.5\,\mathrm{m\,s^{-1}}$).

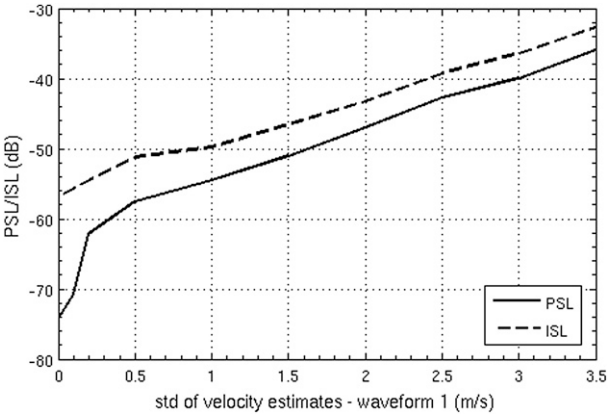

FIG. 6. Sidelobe level as a function of the accuracy of the first pulse Doppler estimates. Input Doppler is $10\,\mathrm{m\,s^{-1}}$ at all range gates.

cells due to the sidelobe problem. Therefore, in designing a pulse compression filter for weather radar, the Doppler effect needs to be taken into account.

Let f_i be the Doppler shift corresponding to a signal at subpulse gate ith, the Doppler phase shift over a period of T_s is $\theta_i = -2\pi T_s f_i$. At the receiver, the transmit waveform is modified to include this Doppler shift,

$$\mathbf{w}^i = (w_0, w_1 e^{j\theta_i}, \ldots, w_{N-1} e^{j(N-1)\theta_i}); \quad j = \sqrt{-1} \tag{20}$$

and

$$\mathbf{W}^i = (\mathbf{w}^i)(\mathbf{w}^i)^{\mathrm{H}}. \tag{21}$$

Accordingly, $\mathbf{W}_k$ needs to be replaced by its Doppler-modulated version,

$$\mathbf{W}_k \rightarrow \mathbf{W}_k^D = \mathrm{circ}[\mathbf{W}^{(n+k)}, k]. \tag{22}$$

4. SES dual-waveform scheme

SES processing requires knowledge of the signal power and Doppler shifts, which are unknown. To tackle this problem, SES proposes a transmission scheme that utilizes two different waveforms. The two waveforms are transmitted separately either in time or in frequency but they both measure the same precipitation volume. Figure 3 depicts that scheme.

In the scenario where the two waveforms can be transmitted simultaneously at different frequencies, the observed volume is perfectly matched. If the two waveforms are transmitted at different times, then the time difference selected should be small enough to ensure that the precipitation volume can be assumed to be statistically stationary. For instance, the two waveforms can be transmitted in a sequence (Fig. 3a); the difference in transmission time between the two waveforms is equal to the dwell time for the first waveform, which is normally on the order of milliseconds. With the different time periods, precipitation targets can be assumed to be unchanged.

The main idea of SES is that the first waveform is used to obtain initiative knowledge of the medium and the second waveform uses this information to deploy SES processing. In detail, the first waveform provides the density distribution and Doppler shift profile of the medium. Using power samples and Doppler samples from these profiles, we generate the adaptive filter [Eq. (19)] for the second waveform. The filter is specified at each range gate. It is noticed that the power samples from the first waveform are independent if the range spacing between them is greater than or equal to the range resolution. Therefore, in designing the second waveform, it is suggested to constrain the second waveform bandwidth to be equal to or smaller than the bandwidth of a rectangular pulse that has a pulse width consistent with the range resolution of the first waveform.

a. Waveform design procedure

Depending on system resources, the SES waveforms can be designed to be time diverse or frequency diverse. For a system with limited bandwidth, the two waveforms can be transmitted consecutively. In that way, both waveforms can use the entire system's available bandwidth. In this scheme, the hardware requirement is minimal. Figure 3a illustrates this transmission technique. The major drawback of this method is that it requires a longer dwell time. Therefore, it is not the best choice for fast-scanning systems like electronically scanned phased array weather radars but is very useful for systems such as cloud radars where the targets do not move or evolve quickly while the sensitivity is more critical. In a system whose bandwidth is

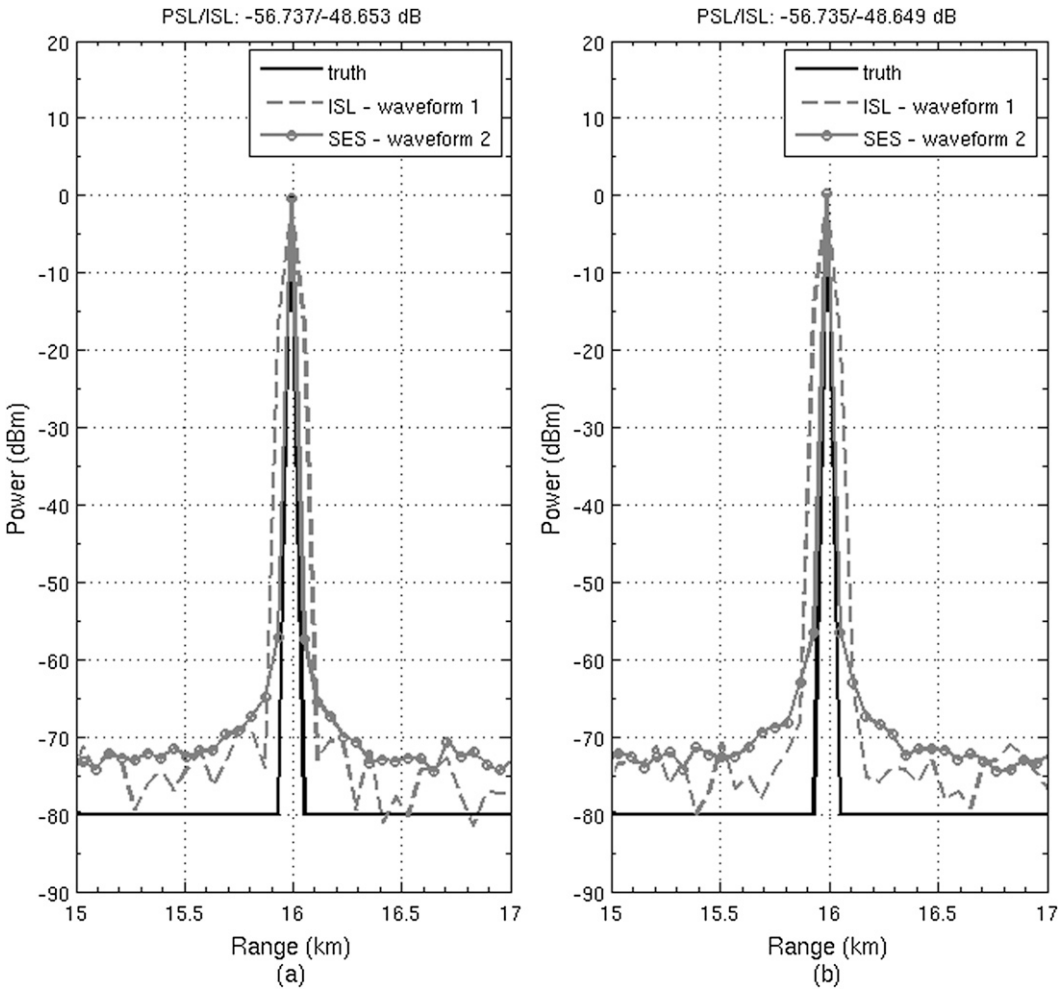

FIG. 7. Sidelobe performance of SES with phase noise of 0.25° and (a) $v = 0\,\mathrm{m\,s^{-1}}$ and (b) $v = 21\,\mathrm{m\,s^{-1}}$.

large enough, the two waveforms can be designed so that their bandwidths are fitted within that band (Fig. 3b) (e.g., the NASA D3R system; Chandrasekar et al. 2010). Volume matching in this case is perfect and dwell time is reduced by half compared to the previous scheme. However, the cost is that the system needs more hardware components and computation power. Each scheme has its own advantages and disadvantages, but SES implementation is flexible enough to fit the design space of most radar pulse compression systems. In general, SES waveform design includes the following steps:

1) Assign the first waveform frequency and bandwidth given the available resources of the system.
2) Determine the waveforms' durations. The first waveform duration is chosen so that it is able to provide adequate PSL performance for weather targets (e.g., −50 dB). Again, the selection depends on the system specifications (e.g., transmitter duty cycle), the design domain (time or frequency domain), and other factors such as the system's blind range requirement. Note that the blind ranges of the waveforms will determine the region where SES processing can be applied.
3) Design the first waveform and its pulse compression filter. At this step, the objective is to acquire moderate PSL and range resolution performance at the output of the first waveform.
4) Compute the range resolution of the compressed pulse of the first waveform.
5) Determine the second waveform's bandwidth. This depends on the desired range resolution and sensitivity of the final output (section 5e). If possible, this bandwidth is chosen to be equal to or smaller than the inverse of the range resolution of the first waveform.
6) Design the second waveform with parameters specified in steps 2 and 5.

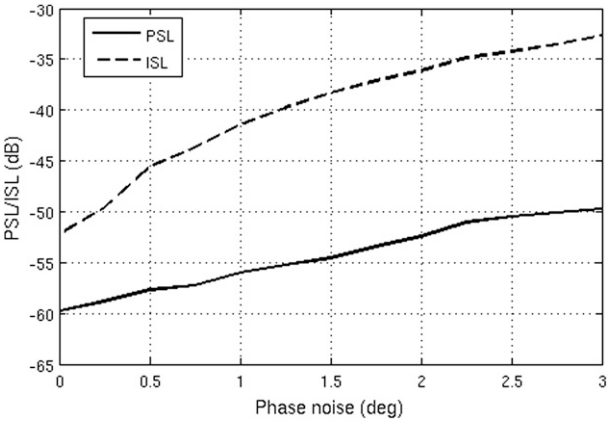

FIG. 8. Peak sidelobe level and integrated sidelobe level as function of the system phase noise.

b. Result combination

In SES processing, there are products available from the two waveforms. Output from the second waveform is expected to have better sensitivity and it is able to measure weak signals more accurately. However, at regions with strong returns, both waveforms should be able to provide comparable measurements. The products are independent because they come from two different waveforms; therefore, they can be arithmetically averaged to generate final results that have lower standard deviations.

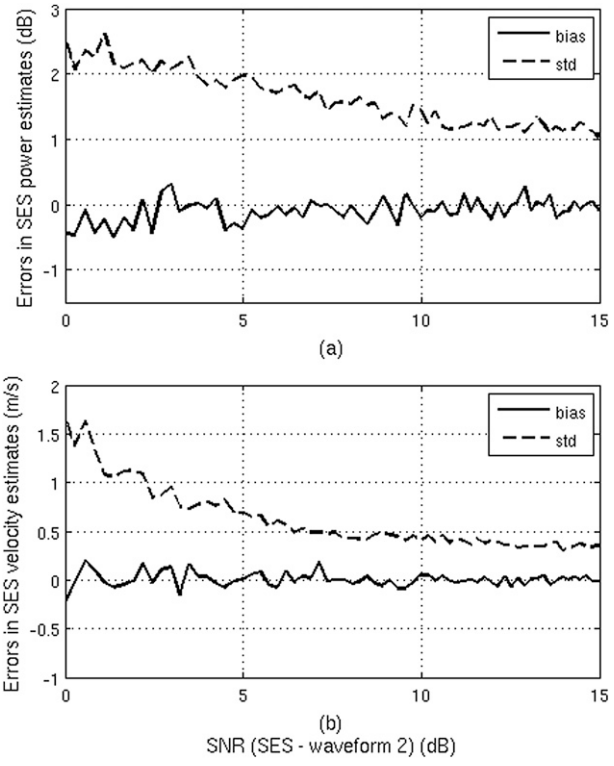

FIG. 9. Bias and standard deviation of SES (a) power and (b) mean Doppler velocity estimates as a function of the SNR with respect to the SES waveform.

5. Method evaluation using simulation

a. Pulse compression weather radar data simulation

To validate the performance of the sensitivity enhancement system developed in this chapter, pulse compression radar signals are simulated for a variety of observation scenarios. Input profiles for the simulation are either synthesized profiles or actual measurements by the Collaborative Adaptive Sensing of the Atmosphere Integrative Project 1 (CASA IP1) radars. The simulation method is done similarly to the procedure described in Mudukutore et al. (1998), except that the effect of the Doppler shift (section 3d) is added. To evaluate the sensitivity improvement, we chose two waveforms have the same width, which is 40 μs. The first waveform's bandwidth is set at 3.6 MHz to provide an adequate peak sidelobe level when using a conventional mismatched filter. The second waveform is computed using the procedure described in the above section. Other input parameters for the simulation are given in Table 1.

b. Minimum ISL filter

The minimization of integrated sidelobe level (ISL) is an efficient technique for designing a mismatched pulse compression filter (Baden and Cohen 1990). Cilliers and Smit (2007) generalized this method by extending the least squares minimization to the L_p norm sense. The filter design is based on the observation that if the input signal is an impulse, then the compressed pulse is the convolution of the transmit waveform and the pulse compression filter. If the compressed pulse's peaks are predefined and are removed from the output, then the remainder coefficients are considered as sidelobe components. An optimization procedure is formed where the cost function is the integrated sidelobe. Solving the optimization problem provides the ISL filter's coefficients. The solution has a closed-form expression; therefore, the design of the filter is very fast and effective. The minimum ISL filter has been shown to be excellent for weather radar applications (Bharadwaj and Chandrasekar 2012). In this work, an ISL filter is used for the first SES waveform.

c. SES range sidelobe performance

When SES is primarily designed to improve the system sensitivity of a pulse compression weather radar, it needs to perform well in other aspects. First, SES should provide a good range sidelobe performance

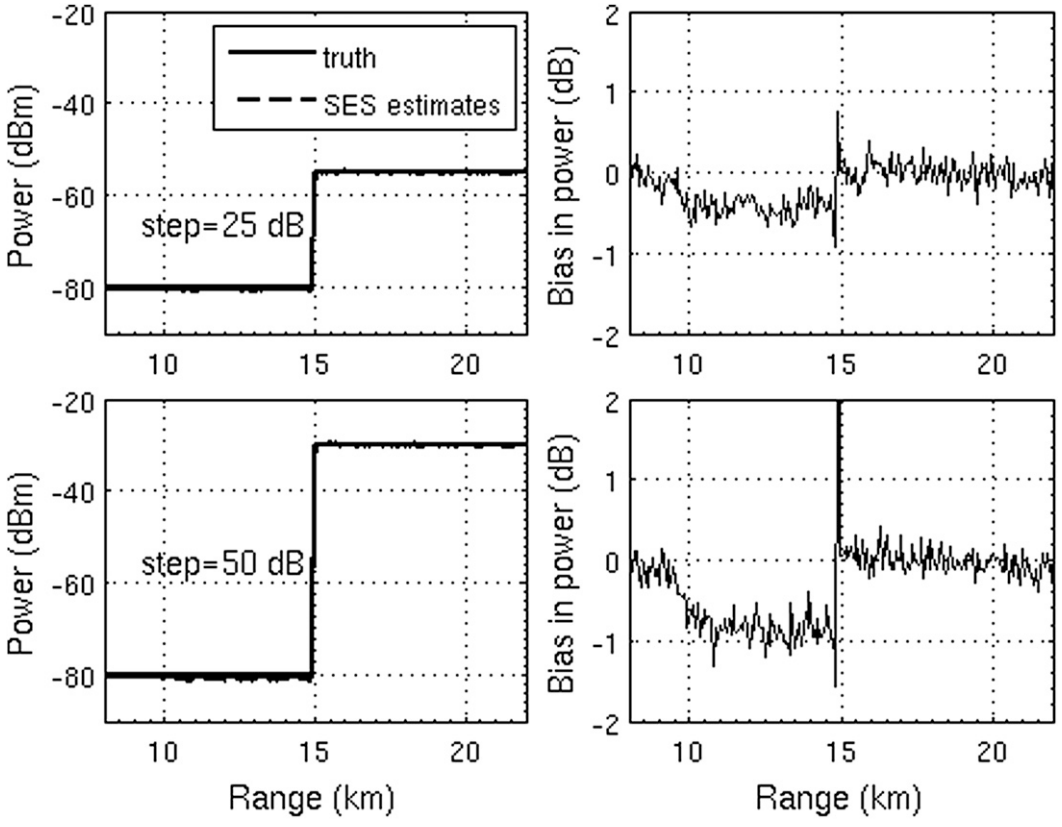

FIG. 10. Step function power profiles with (left) 25- and 50-dB steps and (b) bias in SES power estimates.

because this property is very important for a pulse compression weather radar system. Radar measurements often show strong and steep gradients in the range power profile. Strong echoes may contaminate the nearby range gates via their sidelobes, resulting in large measurement biases. In this experiment, the analysis is carried out with a simulated spike-shaped range power profile that allows us to control the power gradient level. Estimates from the first waveform using an ISL filter will be averaged in range and downsampled to have the same range resolution as that from the second waveform.

The range sidelobe performance of SES is mainly governed by the Doppler shift of the medium, the accuracy of the first pulse Doppler estimates, and the phase noise of the system. Along with the range power profile, a uniform range velocity profile of $10\,\mathrm{m\,s^{-1}}$ is used. In Fig. 4a, when the true power and Doppler velocity profiles are processed as prior information, SES estimates (dark gray line) match perfectly with the inputs and the sidelobe performance in this case is very high. However, when the true power profile is used but the Doppler compensation technique (section 3d) is not implemented, the peak sidelobe level and integrated sidelobe level increase significantly (light gray line). This example demonstrates that SES sidelobe performance is very sensitive to the input Doppler profile and that it is necessary to use Doppler compensation in SES. In Fig. 4b when input power and Doppler profiles are obtained from the first waveform, SES results are not as perfect as the case using true profiles but still very good. The SES sidelobe level due to Doppler shift is shown as a function of mean velocity in Fig. 5. The PSL and ISL are about -60 and -50 dB, respectively, and almost invariant with velocity within the Nyquist range ($v_a = 21.5\,\mathrm{m\,s^{-1}}$). Above the Nyquist velocity, velocity aliasing happens at the first waveform and, consequently, SES sidelobe-level performance decreases quickly. Figure 6 shows the dependence of the SES sidelode level when there is increasing error in the first pulse Doppler estimates. The accuracy of the mean Doppler velocity estimate is determined by many factors, such as the intrinsic spectrum width of the scatterers, the number of integration samples (N), and the SNR. For a Ku-band radar system with $\lambda = 2.16$ cm, pulse repetition time (PRT) $= 0.25$ ms, $N = 128$, and spectrum width of $2\,\mathrm{m\,s^{-1}}$, the mean velocity from the first pulse can be estimated with an accuracy of about

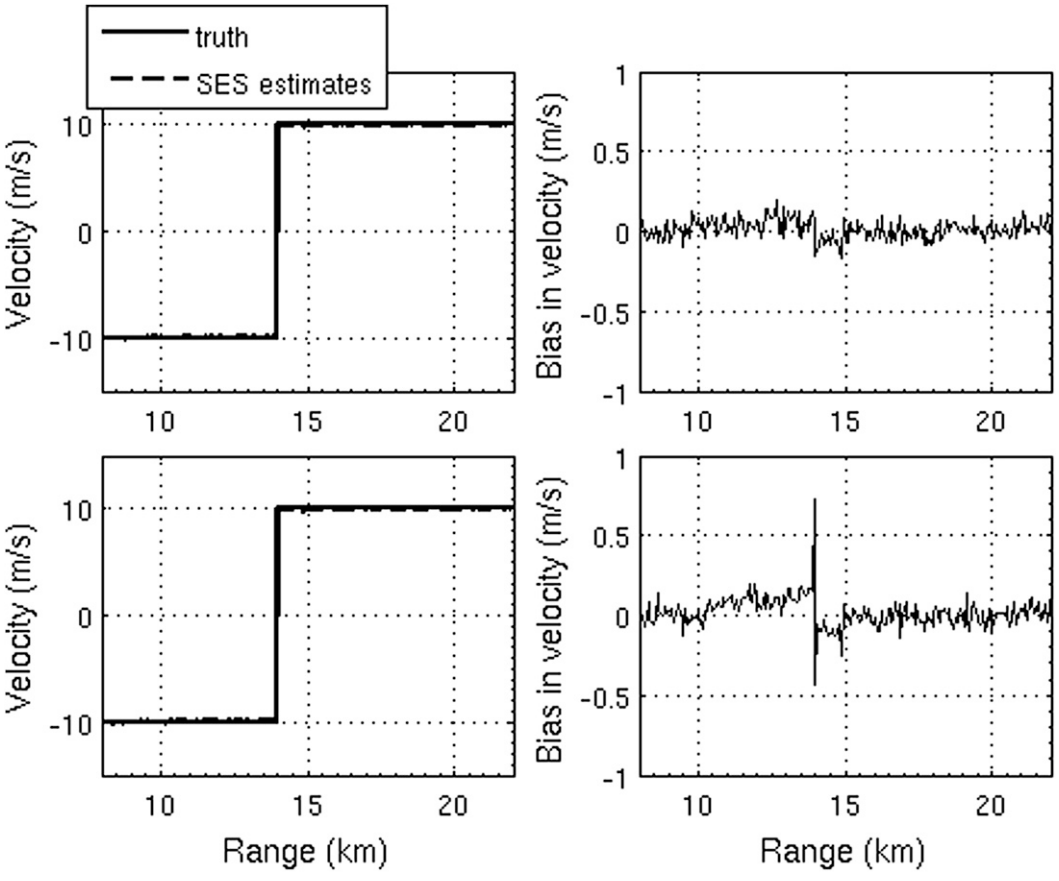

FIG. 11. Range Doppler velocity profiles corresponding to the power profiles in Fig. 10. Input profile to the simulation has (left) a 20 m s^{-1} velocity step and (right) bias in SES velocity estimates.

1.2 m s^{-1} at SNR = 0 dB. At that accuracy level of Doppler estimate, SES provides PSL and ISL better than −52 and −45 dB, respectively.

In a radar system, the fluctuation in the phase of individual components such as local oscillators, mixers, and transmitters contributes to the system's phase noise. Consequently, the phase of the subpulses of the transmit waveform has random phase errors and it will affect the performance of SES processing. In this work, we assume that the random phase errors of the transmit subpulses are independent and uniformly distributed in the range $[-\alpha, \alpha]$ degree. Examples of sidelobe performance of SES with phase noise of $\alpha = 0.25°$ are shown in Fig. 7. Compared to the results in Fig. 4, the phase noise slightly raises the SES sidelobe level. The PSL and ISL as a function of phase noise are presented in Fig. 8. As expected, both PSL and ISL performance decreases when the phase noise increases. For a system with a phase noise of greater than or equal to 0.5°, SES is able to provide an ISL smaller than or equal to −45 dB.

d. *Doppler spectral moments estimation accuracy*

The second consideration of SES performance is power and velocity measurement accuracy. The SES system is designed to achieve an advantage when the signal is weak. It is necessary to illustrate the SES bias and standard deviation of the moment estimates at a low signal-to-noise ratio (SNR < 10 dB). In this analysis, a Gaussian-shaped profile of the reflectivity is used to simulate the range profile. The high SNR of the profile is 15 dB, and the SNR of the floor of the profile is −5 dB with respect to the SES waveform. Figure 9 shows the simulation results with $N = 128$ pulses. The simulations were repeated 100 times for the same reflectivity profile to generate statistical plots. Figure 9a shows the bias and standard deviation of estimated reflectivity from the SES waveform. It can be seen that SES performs well as estimated reflectivity is unbiased when SNR > 3 dB; at lower SNRs, SES exhibits slightly negative biases but they are within a limit of −0.5 dB. The standard deviations behave as expected; it is about 1 dB at high

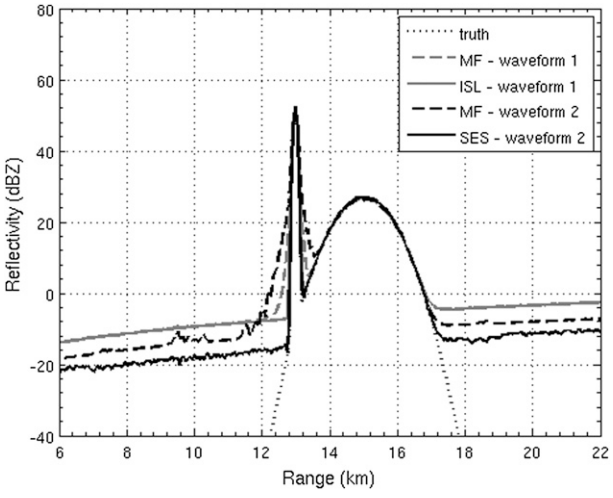

FIG. 12. Synthesized reflectivity profile (dotted line) simulating ground clutter and precipitation echoes and results from different pulse compression filters. Floor of the true profile is set well below the noise floors of the filters for sensitivity analysis. SES filter shows the best performance in terms of sensitivity.

SNRs and increases when the signal becomes weaker. For velocity (Fig. 9b), SES provides unbiased estimates at all SNR values.

Next, instead of using a Gaussian-shaped echo profile, a step function profile with different step sizes is used to study the effects of very high gradients in the power profile within the long pulse. The power of the signals on either side of the gradient differs by 25 and 50 dB, respectively, and the mean Doppler velocity changes from -10 to $10\,\mathrm{m\,s^{-1}}$. Figure 10 shows the observed power profile by SES and the bias in the estimated power. It can be observed that negative biases in power only occur at the weak signal region near the gradient. This can be explained by the presence of strong signals in the SES deconvolution process. At a step size of 25 dB, the bias in power is within acceptable levels of ± 0.5 dB. The bias is larger at a step size of 50 dB, but this is an extreme case and rarely happens in a practical range power profile. For velocity estimates, SES does not bias the measurement more than $0.2\,\mathrm{m\,s^{-1}}$ in either case (Fig. 11). In summary, SES performs very well in Doppler spectral moment estimation. This is attributed to its excellent performance in sidelobe and Doppler tolerance.

e. *SES sensitivity gain*

The main contribution of SES is to provide a better sensitivity performance than conventional filter systems. In this section, an extensive analysis is performed to evaluate SES in this aspect. To assess the improvement in sensitivity, we define the SES sensitivity gain as the difference in sensitivity between the outputs of SES and a matched filter for the first waveform. Minimum detectable reflectivity of the system using a matched filter for the first waveform is computed based on Eq. (10). For SES, since the filter coefficients change at each range gate, we cannot apply Eq. (10) directly. Thus, the sensitivity curve is obtained by means of simulation. To do that, a profile containing only a receiver noise signal is used as the input for SES. The output profile is the sensitivity curve for SES.

The first experiment is carried out with a simulated reflectivity profile consisting of two Gaussian-shaped echoes. The narrow echo with high power mimics the return signals from ground clutter and the other simulates a weather echo. The floor of the profile is set well below the noise floor of the filters to study the filters' sensitivity levels. Again, a uniform mean Doppler velocity profile of $10\,\mathrm{m\,s^{-1}}$ is used. Along with SES and the ISL filter, a standard system using a matched filter (MF) for both waveforms is also implemented for comparison. In Fig. 12, the ISL filter for the first waveform (solid dark gray line) performs pretty well. The sensitivity is matched to that of the matched filter (dashed dark gray line) and the PSL performance is improved. Among those conventional filters, the matched filter for the second waveform (light gray line) has a better sensitivity because of its smaller bandwidth; however, its PSL performance is by far the worst. This is expected for a matched filter for a waveform with a time bandwidth product (BT) of only 100. For this filter, the observed weather echo is heavily contaminated by the sidelobes from the ground clutter and therefore, the MF system for the second waveform does not meet the requirements for pulse compression weather radar and cannot be used in practice. On the other hand, SES (solid black line) shows the best performance in both sidelobe and sensitivity aspects. The sensitivity curves of the matched filter for the first waveform and SES for the second waveform implies an improvement of 7.8 dB in sensitivity for SES.

The analysis of the performance of SES thus far was done using synthetic profiles for reflectivity, velocity, SNR, etc. These profiles show the performance of SES in extreme conditions and provide a worst-case analysis. It is interesting to observe the behavior of SES with real weather profiles; to do that we ran SES on pulse compression–simulated data where inputs were generated from data collected by CASA IP1 Cyril radar during a tornado event in Oklahoma on 10 February 2009. The only modification here is that the power profiles are lowered for the purpose of studying sensitivity. All other moment profiles were retained as in the original data. The profiles were sampled at azimuth

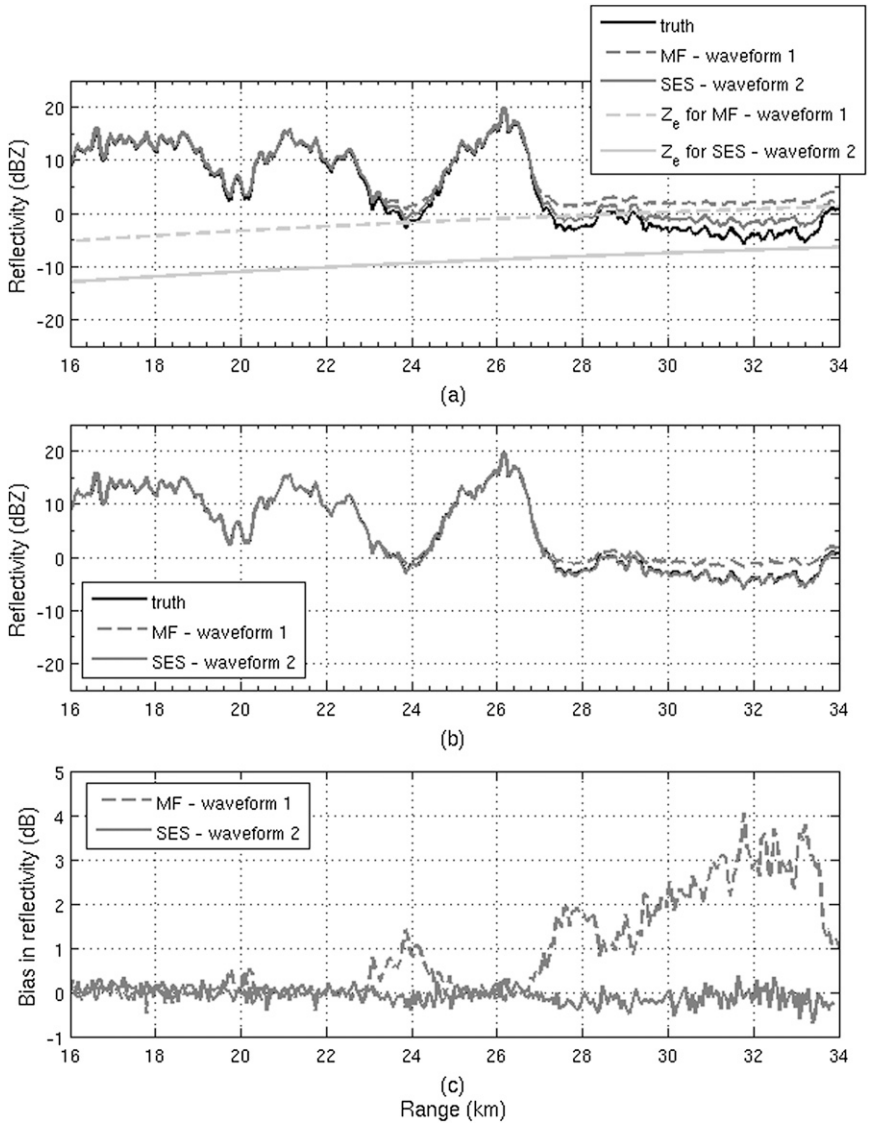

FIG. 13. Cyril radar reflectivity profile at azimuth 330° (lowered by 20 dB for sensitivity analysis). (a) Measured reflectivity profiles by MF (waveform 1) and SES (waveform 2), (b) reflectivity estimates after noise suppression, and (c) bias in reflectivity estimates. Sensitivity curves (Z_e) for both systems are also superimposed for comparison.

330° of the plan position indicator (PPI) presentation of the scan. In Fig. 13, power profiles are 20 dB less compared to the measurements. The top panel shows the input reflectivity profile (solid black line), measured reflectivity from SES (solid dark gray line), and MF for the first waveform (dashed dark gray line). For a fair comparison of power biases at low SNR, the noise needs to be removed from the measurements in both systems (MF and SES). The middle panel depicts results from SES and MF after subtracting noise powers from measured profiles in Fig. 13a. In the bottom panel, biases in the reflectivity estimates are shown. The minimum sensitivity curves for both systems are generated and superimposed on the plots for comparison. At regions with strong echoes (e.g., a range from 16 to 19 km), SES and MF performance are comparable. Both systems are capable of providing accurate measurements. However, when the signal strength decreases (e.g., at a range from 23 to 25 km), the matched filter starts showing large power biases because of its lower sensitivity and SES still performs well.

In the next experiment, we reduce the input powers further (by 35 dB), so that the input reflectivity profile is below the sensitivity curve of the MF system for the first waveform at almost the whole range (Fig. 14a). The results in Fig. 14c show that the MF system for the first

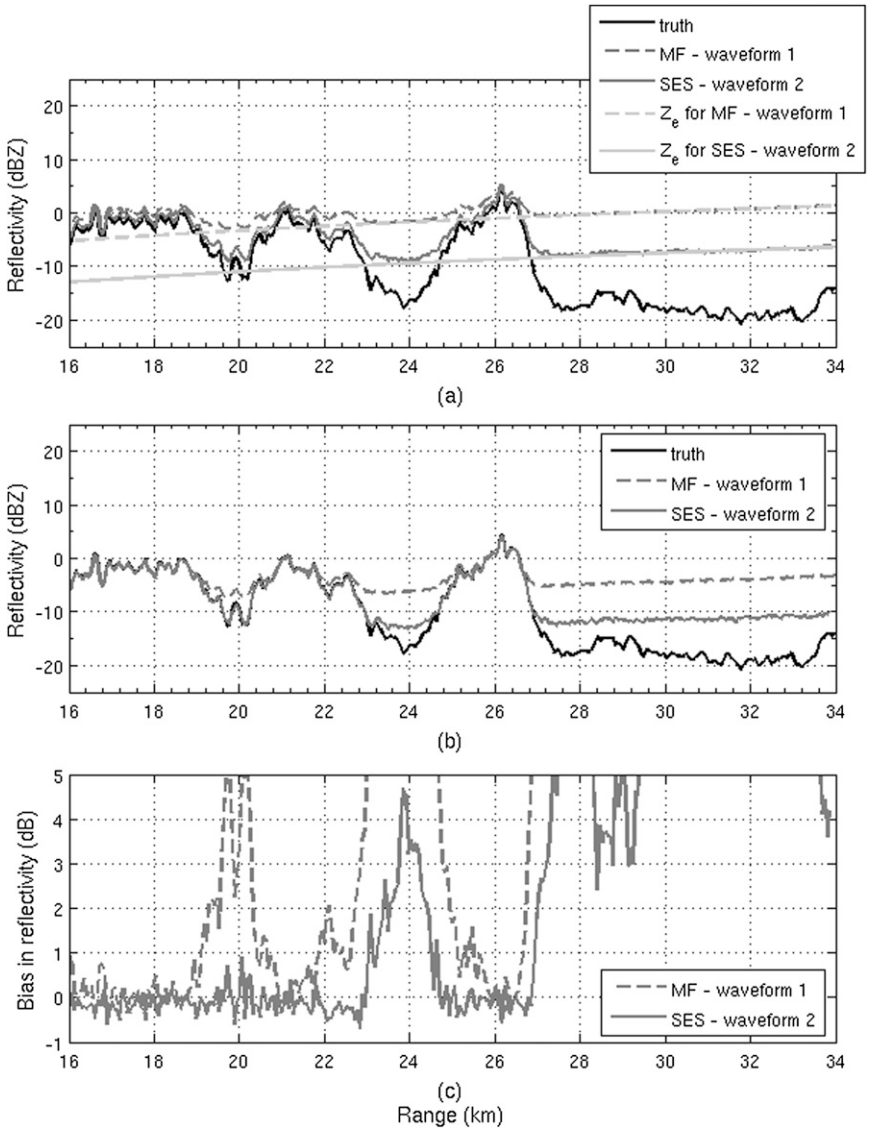

FIG. 14. As in Fig. 13, but the input reflectivity profile was lowered by 35 dB.

waveform fails to estimate the signal. Its power biases are from 3.5 to 15 dB at all range gates. In contrast, SES still works fairly well. Because of the lower SNR, the bias performance is slightly worse compared to that in Fig. 13c. However, at the regions where the signal is above the SES sensitivity curve, the SES power biases are within the ±0.5-dB limit. It is recalled that SES deploys information about the medium extracted from the first waveform outputs, which in this case is off by a large margin. Hence, this analysis demonstrates that SES is a very stable and robust method.

The sensitivity improvement in SES processing is governed by many factors, such as pulse lengths and bandwidths of the two pulse compression waveforms. Given two waveforms with an identical pulse width (40 μs) and bandwidths of 3.6 and 2.5 MHz (Table 1), the SES sensitivity gain is 7.8 dB. Different configurations of the pulse compression waveforms and filters produce different SES sensitivity gains. In general, increasing the pulse width and/or reducing the bandwidth of the second waveform results in better sensitivity improvement. The next section demonstrates this idea using actual data from the NASA D3R radar.

6. Illustration with NASA D3R Ku–Ka system observations

The objective of the NASA D3R system is to provide ground-based measurements for cross validation with the precipitation observations of the Global Precipitation

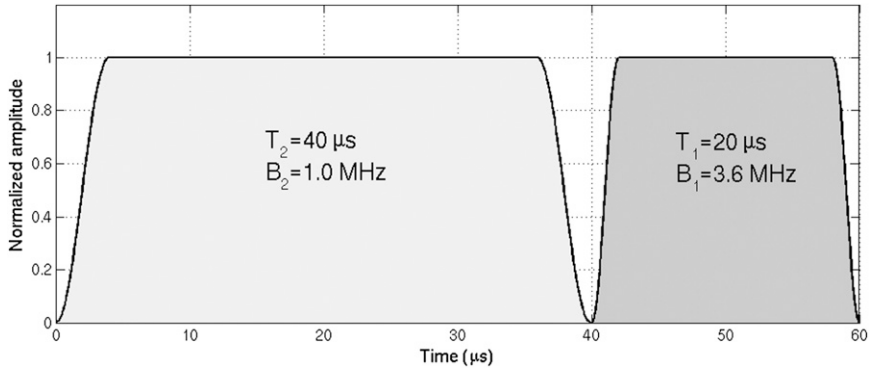

FIG. 15. Waveform scheme for the SES experiment on the D3R system.

Measurement (GPM) program (Chandrasekar et al. 2010). To enable measurements for light rain and snow, the radar employs frequencies in the Ku and Ka bands. For both of these highly attenuating frequencies, the required sensitivity of the D3R is pegged at −10 dBZ at 15 km for a single pulse measurement in clear air. The radar also has a requirement of measuring Doppler velocity up to 25 m s^{-1}; to enable this, it operates in the staggered PRT 2/3 mode. With such a premium placed on its sensitivity, the D3R system is an appropriate platform for testing the efficiency of the SES waveform.

In its normal operational mode, the D3R employs a novel frequency diversity waveform (Bharadwaj et al. 2009) consisting of three subpulses of durations 40 (long), 20 (medium), and 1 μs (short). The long and medium pulses are each coded with the signal bandwidth of 3.6 MHz. For transmission, this waveform is upconverted from a baseband sample rate of 50 MHz. The digital receiver subsamples the received waveform at 200 MHz and then processes the downconverted data through a pulse compression filter that has an output sample rate of 10 MHz (Chandrasekar et al. 1986). The in-phase (I)

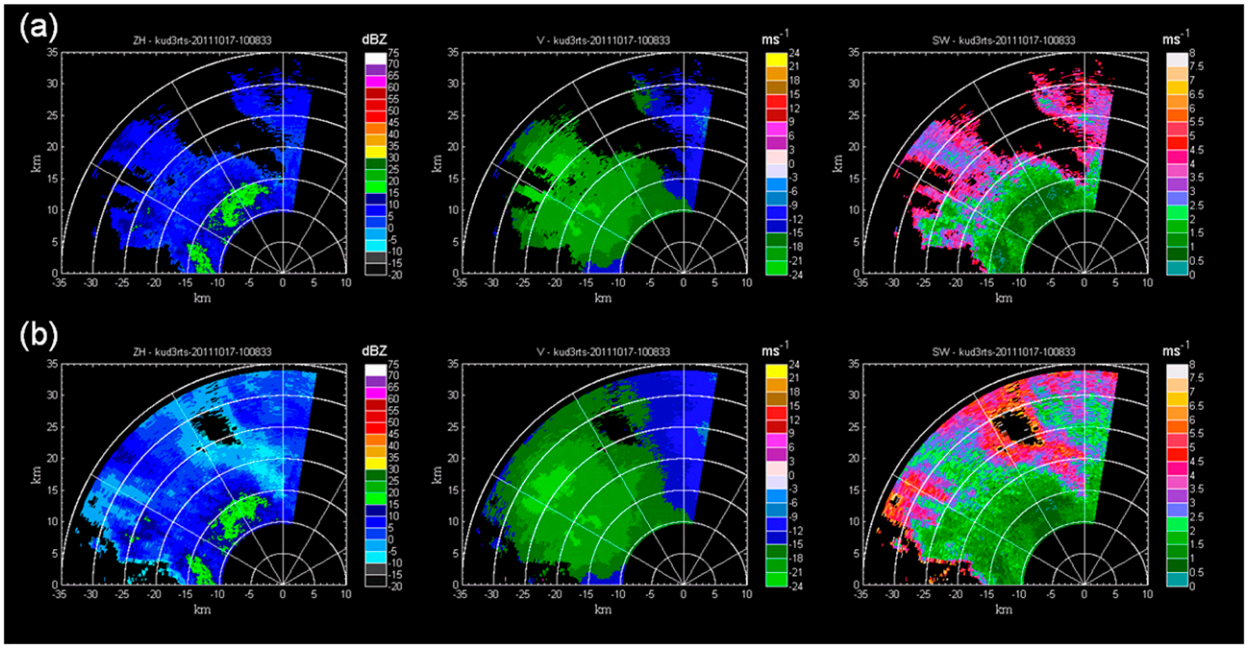

FIG. 16. Sector PPI images of (left) reflectivity (H polarization), (middle) velocity, and (right) spectrum width during a light rain event observed by the D3R system. Data are masked using a threshold of SNR > 0 dB. (a) A 3.6-MHz bandwidth medium pulse output processed with a matched filter. (b) Output of the SES system—a 3.6-MHz bandwidth medium pulse processed with an ISL filter as the reference signal for a 1-MHz bandwidth long pulse, coded and processed using the SES algorithm.

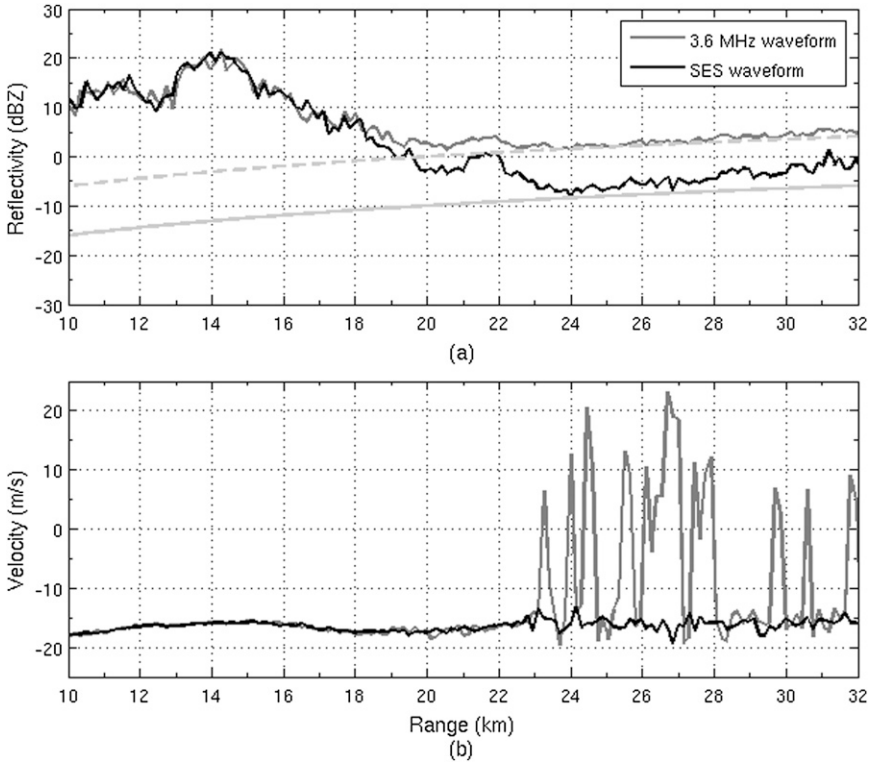

FIG. 17. Sample profile at azimuth of 341° from Fig. 16 to show the (a) reflectivity and (b) velocity measurements from SES (solid black line) and the medium waveform of D3R (solid gray line). By using SES, the system sensitivity is improved by 10 dB when compared to that of the conventional matched filter for the medium waveform.

and quadrature-phase (Q) outputs are finally made available at a downsampled rate of 1 MHz.

For the SES experiment on the D3R system, the waveform scheme consisted of only the long and medium subpulses. The pulse durations for the two-pulse SES waveform were kept identical to those of the long and medium pulses of the normal three-pulse D3R waveform (Fig. 15). Further, the measurements obtained by the medium pulse in the SES waveform were used as prior knowledge (the first waveform in the SES scheme). Therefore, the signal bandwidth (=3.6 MHz) of the SES medium pulse was also identical to that of the medium pulse in the regular three-pulse waveform. However, the SES long pulse was designed for 1-MHz bandwidth to match with the current radar configuration. This setup enables a fair comparison between the data corresponding to the two waveforms and maximum compatibility with the normal processing mode of the radar. The SES experiment on the D3R system was carried out on 17 October 2011, during a light rain event. The D3R radar was deployed at the Colorado State University–University of Chicago–Illinois State Water Survey (CSU–CHILL) radar facility at Greeley, Colorado, at the time of the experiment.

Figure 16 shows the Ku-band measurements obtained by the two waveforms during a sector PPI scan. It should also be noted that the total blind range for the long pulse is approximately 9 km when operated in multipulse mode. The first row in Fig. 16 shows the estimates of the signal's first three spectral moments (reflectivity, mean velocity, and spectrum width) from a matched filter for the medium pulse in the SES scheme. The second row shows the outputs of the SES processing. In the weak echo regions such as the 330°–360° sector, it is obvious that the SES processing provides enhanced sensitivity when compared to the medium pulse. Further, the observations made by the SES long and medium pulses show a remarkable agreement in the reflectivity as well as the velocity for the stronger echo regions (region between an azimuth of 300°–345° and a range of 10–20 km).

In Fig. 17, reflectivity and velocity profiles at the azimuth angle of 341° from Fig. 16 are depicted. For the range gates with stronger echoes (such as those present from 10 to 18 km), the outputs of the MF for the medium pulse and the SES algorithm closely agree. At the range gates where weaker signals are exhibited (from 22- to 32-km range), SES performance is superior over the MF

system. SES is able to pick up lower reflectivity and significantly improves the velocity estimates in those range gates. It is shown that, for this setup, SES improves the system sensitivity by 10 dB.

7. Summary and discussion

It is likely that the final goal for electronic scan weather radar technology will include the use of low-power solid-state transmitters at each element of an active array. The main drawback of these transmitters is the lack of high peak power. To meet the requirement of sensitivity for weather observations, a pulse compression technique is used. The conventional matched or mismatched filters for pulse compression waveform have some limitations that partly downgrade the sensitivity. In this paper, a new pulse compression system, SES, is developed to address this problem.

SES deploys a dual-waveform transmission scheme. The two waveforms are related and can be transmitted simultaneously in the frequency domain or consecutively in the time domain. Time spacing between the two waveforms' transmission is kept small to ensure that the precipitation is statistically stationary. Using the knowledge of the precipitation volume extracted from the first waveform, an adaptive filter for the second waveform is designed. The new filter is capable of achieving better sensitivity than the conventional matched filter. The improvement margin depends on the available resource of the system as well as the design output parameters. As demonstrated by radar simulation and actual observations from the NASA D3R Ka–Ku radar, SES is able to enhance the system sensitivity by 7–10 dB. In regions with strong echoes, the results from the two SES waveforms can be combined to reduce the measurement standard deviations. In addition to the improved sensitivity, SES is able to provide very good sidelobe performance and Doppler tolerance. The impact of the system phase noise was characterized for PSL and ISL. It is suggested that a phase noise of 0.5° or better is required to minimize the range sidelobe problem. The impact of a strong gradient in power and mean Doppler velocity range profile is also presented. In most cases, the biases and standard deviation of SES power and mean velocity estimates are within the acceptable limits.

Besides the advantages, SES is computationally intensive. Although the SES adaptive pulse compression filter is defined in a closed-form expression, it needs to be computed at every single range gate. This will increase the computational load of the system considerably. Also, the algorithm in SES requires the information of $(N - 1)$ signals prior to and after each processed gate and it will reduce the range where SES can be applied. Despite these limitations, with its excellent performance, flexibility in waveform design, and especially its capability of improving sensitivity, SES is an attractive technique for pulse compression weather radar.

Acknowledgments. The D3R radar data and analysis are supported by the NASA PMM program. The authors would like to thank Kumar Vijay Mishra for his assistance on implementing SES waveforms.

REFERENCES

Baden, J. M., and M. N. Cohen, 1990: Optimal peak sidelobe filters for biphase pulse compression. *Record of the IEEE 1990 International Radar Conference,* IEEE, 249–252.

Bharadwaj, N., and V. Chandrasekar, 2012: Wideband waveform design principles for solid-state weather radar. *J. Atmos. Oceanic Technol.,* **29,** 14–31, doi:10.1175/JTECH-D-11-00030.1.

——, K. V. Mishra, and V. Chandrasekar, 2009: Waveform considerations for dual-polarization Doppler weather radar with solid-state transmitters. *2009 IEEE International Geoscience and Remote Sensing Symposium: Proceedings,* Vol. 3, III-267–III-270.

Bringi, V. N., and V. Chandrasekar, 2001: *Polarimetric Doppler Weather Radar: Principles and Applications.* Cambridge University Press, 636 pp.

Bucci, N. J., and H. Urkowitz, 1993: Testing of Doppler tolerant range sidelobe suppression in pulse compression meteorological radar. *Proceedings of the IEEE National Radar Conference,* IEEE, 206–211.

Chandrasekar, V., V. Bringi, and P. Brockwell, 1986: Statistical properties of dual-polarized radar signals. Preprints, *23rd Conf. Radar Meteorology,* Snowmass, CO, Amer. Meteor. Soc., 193–196.

——, M. Schwaller, M. Vega, J. Carswell, K. V. Mishra, R. Meneghini, and C. Nguyen, 2010: Scientific and engineering overview of the NASA dual-frequency dual-polarized Doppler radar (D3R) system for GPM ground validation. *2010 IEEE International Geoscience and Remote Sensing Symposium,* IEEE, 1308–1311.

Cilliers, J. E., and J. C. Smit, 2007: Pulse compression sidelobe reduction by minimization of L_p -norms. *IEEE Trans. Aerosp. Electron. Syst.,* **43,** 1238–1247, doi:10.1109/TAES.2007.4383616.

Fetter, R. W., 1970: Radar weather performance enhanced by compression. Preprints, *14th Conf. in Radar Meteorology,* Tucson, AZ, Amer. Meteor. Soc., 413–418.

Keeler, R. J., 1995: Pulse compression waveform analysis for weather radar. *COST 75—Weather Radar Systems: International Seminar,* C. G. Collier, Ed., European Commission, 603–614.

Mudukutore, A. S., V. Chandrasekar, and R. J. Keeler, 1998: Pulse compression for weather radars. *IEEE Trans. Geosci. Remote Sens.,* **36,** 125–142, doi:10.1109/36.655323.

RCA, 1965: Optimum waveform study for the coherent pulse Doppler. Office of Naval Research, Department of the Navy Tech. Rep. AD-641-391, Contract NONR-4649(00)(X), 252 pp.

Skolnik, M. I., 2002: *An Introduction to Radar Systems.* McGraw-Hill, 772 pp.